Materials & Design 219 (2022) 110769

Contents lists available at ScienceDirect

Materials & Design

journal homepage: www.elsevier.com/locate/matdes

Role of GNDs in bending strength gain of multilayer deposition generated heterostructured bulk aluminum

Xihang Zhao [a], Zhenming Yue [a,*], Ge Wang [b], Zan Li [b], Celal Soyarslan [c]

[a] School of Mechanical, Electrical and Information Engineering, Shandong University at Weihai, Weihai 264209, China
[b] State Key Laboratory of Metal Matrix Composites, Shanghai Jiao Tong University, Shanghai 200240, China
[c] Chair of Nonlinear Solid Mechanics, Faculty of Engineering Technology, University of Twente, 7500AE Enschede, The Netherlands

HIGHLIGHTS

- The introduction of gradient structure brings the inhomogeneous deformation among different layers, and the induced strain gradient can achieve the purpose of work hardening.
- GNDs accumulation can be observed at the interface of two different ratio components.
- The addition of the number of gradient cycles enables the material to get another large-scale strain gradient across the microstructure.

GRAPHICAL ABSTRACT

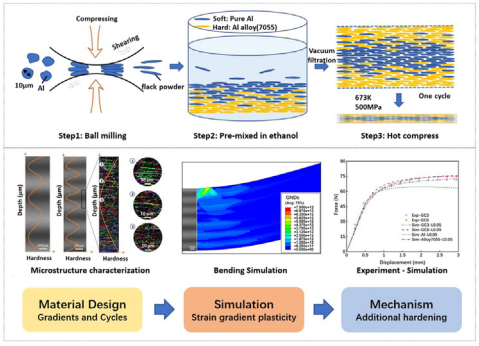

ARTICLE INFO

Article history:
Received 10 March 2022
Revised 18 May 2022
Accepted 18 May 2022
Available online 21 May 2022

Keywords:
Strain hardening
Strain gradient
FEM
Heterostructure

ABSTRACT

Gradient structured materials have been proven to have excellent mechanical properties, such as strength–ductility synergy and excellent strain hardening. In this study, the deformation mechanism of heterostructured bulk aluminum with submicron deformation mechanisms was investigated using a mechanism-based strain-gradient plasticity model, whose gradient information was obtained using a discrete gradient computation method. The model was then used to simulate bending of the material and investigate extra strain hardening. The microstructure of the material was characterized using electron backscattered diffraction analysis. The complicated dislocation reactions occurring during the deformation of multilayer deposition material were determined from the simulation results. The distribution and evolution of geometrically necessary dislocations (GNDs) were numerically determined. The simulation results demonstrate that the GNDs and the number of material gradient cycles have a direct influence on plastic hardening. Inclusion of more layer periods in the material resulted in additional large-scale strain gradient across its thickness. The results of this study advances the understanding of the underlying deformation mechanisms that control ductility and strengthening over periods and gradients and provides the possibility of obtaining multilayer materials with exceptional mechanical properties.

1. Introduction

The trade-off between strength and ductility has always been a challenging problem in material science. Numerous attempts have been made through microstructure design to realize the synergy

* Corresponding author.
E-mail address: yuezhenming@sdu.edu.cn (Z. Yue).

https://doi.org/10.1016/j.matdes.2022.110769
0264-1275/

between these two mechanical properties. Gradient-structured metals show excellent performance in this respect [1,2]. The structural gradient results in a plastic strain gradient [3–5], which can result in many advantages, such as higher strength [6,7] and ductility [8], good fatigue resistance [9]. Gradient nanograined (GNG) materials, in which the grain size gradually varies from a few nanometers at the surface to a few microns inside the matrix, have shown excellent strength–plastic synergy [7]. For example, the yield strength of GNG copper bars is about 130 MPa, twice that of coarse-grained (CG) copper bars, and maintaining a ductility of approximately 30% [10]. By introducing a gradient structure into an interstitial-free (IF) steel sheet, its yield strength is 1.6 times higher than its CG counterpart while the elongation is unhindered [11]. These results show that the unique microstructure of gradient structure metals results in an excellent strength–ductility synergy [12–14].

Upon plastic deformation, stress and strain heterogeneity mediated by structural gradients activate new dislocation mechanisms, which in turn lead to size-dependent strengthening of the material [15]. From a microscopic perspective, the plastic deformation of metals is characterized by the formation and aggregation of a large number of dislocations. There are two different manifestations of dislocations [16]: statistically stored dislocations (SSDs), which evolve from random trapping processes during plastic deformation, and geometrically necessary dislocations (GNDs), which appear in strain gradient fields due to geometrical constraints of the crystal lattice. Owing to the gradient distribution of the phase, nonuniform deformation occur at different levels during the deformation process. The incompatibility of hard-zone and soft-zone deformations in a material leads to gradients during plastic deformation [17]. In Fig. 1a [14], GNDs emanate from Frank–Read sources within the soft region and pile up at its boundary with an adjacent hard region. In the soft zone, these dislocations create long-range back stress that prevents glide of the trailing GNDs; thus, significantly strengthening the soft zone. The back stress is in the direction opposite to that of the applied stress. In addition to this, the accumulation of GNDs produces a concentrated forward stress at the zone boundary, which is opposite to the back stress. At the boundary of the region, the backward and forward stress cancel each other. This improves the yield strength of the heterogeneous material, while an increase in the internal stress after yield results in strain hardening that retains or even improves plasticity [18]. In addition to the microstructure, the strain gradient in the material is also closely related to the loading condition. Metals exhibit strong strain gradient plasticity during non-uniform plastic deformation such as bending [19,20], torsion [21], and indentation [22]. For example, during bending, the dislocation density is directly related to the gradient of plastic deformation with distance. As shown in Fig. 1b [16], a gradient of slip $\partial\gamma_\alpha/\partial x_1$ along the x_1 direction on the α slip system results in the formation of GNDs with their density given by $\rho_G = \frac{1}{b}\left(\frac{\partial\gamma_\alpha}{\partial x_1}\right)$, where b is the Burgers vector.

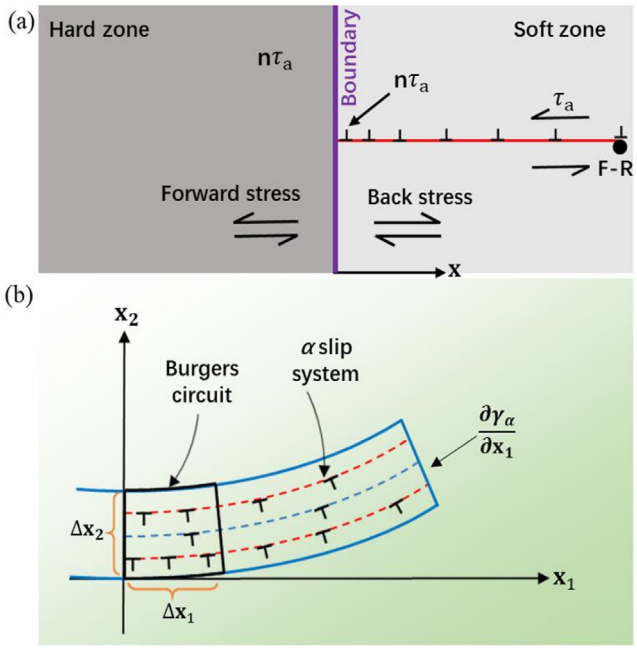

Fig. 1. Schematic of two sources of geometrically necessary dislocations: (a) piling up of geometrically necessary dislocations in the soft zone producing back stress in the soft zone and forward stress in the hard zone [14], (b) a gradient of slip on the α slip system along the x_1 direction causes storage of geometrically necessary dislocations [16].

Physically based constitutive models are often used to study the effects of multiple mechanisms on the mechanical behavior of materials. The rule of mixtures (ROM) has been applied in the field of composite materials to obtain the mechanical response of gradient-structure materials [23,24]. However, Zhu et al. [17] have shown that heterogeneous materials exceed ROM because of the excellent synergies delivered by the heterogeneous regions. Finite element simulations can be used in gradient-structure materials by adding constraints between the multiple regions [25,26]. However, GNDs caused by nonuniform deformation are often ignored. Zhang et al. [27] introduced a scalar measure of the plastic strain gradient into the hardening rate and, based on a simplified one-dimensional gradient theory, verified that the additional strength indeed depended on the plastic strain gradient. However, the mechanical mechanism of gradient plasticity between different components and the direction of the gradient have not been clearly explained.

In this study, heterostructured aluminum with a controllable gradient structure was prepared using the powder assembly method, as shown in Fig. 2a. To validate our design concept and explore the role of GNDs in the strength gained by multilayer deposition-mediated heterostructured bulk aluminum. Mechanism-based strain gradient plasticity (MSGP) [28] was adopted, which can reflect the strengthening of strain gradient caused by heterogeneous structure on material deformation. The mechanical response and deformation characteristics of multi-period heterostructured bulk aluminum (Al/7055) under bending conditions were studied. Since the sample is not melted during preparation. Therefore, additional hardening caused by segregation precipitation of the second phase was ignored in this study. Metals with a gradient structure exhibit higher gradient plasticity when deformed under a bending load [19,20]. It was found that the gradient structure has a particular influence on the deformation behavior of the components, which is mainly caused by the internal stress generated by heterogeneous deformation. The validity of the finite element model was verified by comparing it with experimental results. The gradient plasticity simulations thus performed provides insights in the exploration of strength gradient optimization.

2. Theoretical aspects

The classical elastic–plastic theory only considers SSDs and not GNDs. The deformation-compatible GND mechanism primarily controls the size-effect of the material, and the GND density is related to the strain gradient. In the following, we present the building blocks of MSGP in the lines of [28,29].

2.1. MSGP hardening model

According to the Taylor dislocation model, the relationship between shear flow-stress τ and dislocation density ρ can be expressed as [16].

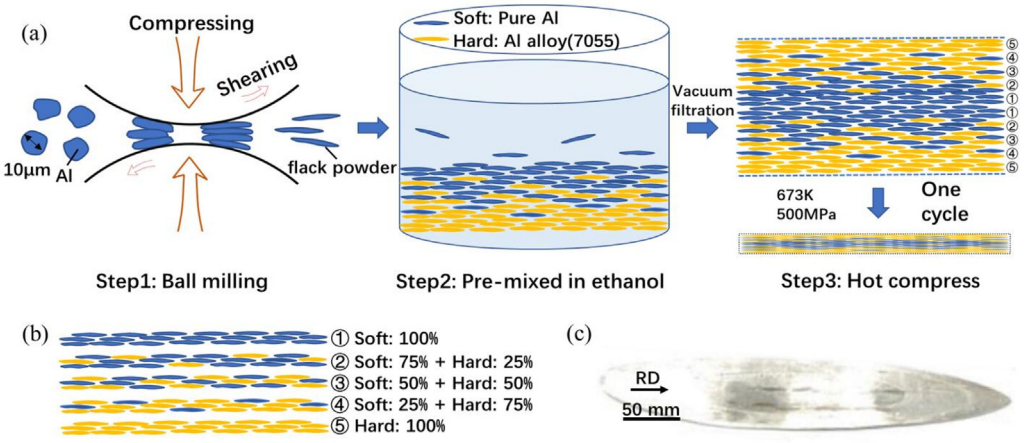

Fig. 2. Design of heterostructured bulk Al with controllable gradient structure. (a) Schematic of the fabrication process. Different ratios of Al/Al alloy flaky powders are pre-mixed in an ethanol solution, followed by vacuum filtration, and finally hot-pressed at 500 MPa (at 673 K). (b) Different ratios of Al/Al alloy flaky powders. (c) After hot compression, the aluminum sheet was annealed for 2 h (at 723 K) and further hot-rolled (90% thickness reduction at 723 K).

$$\tau = \alpha\mu b\sqrt{\rho} \tag{1}$$

where μ is the shear modulus of the matrix, α is an empirical constant of approximately 0.3 [30], and b is the magnitude of the Burgers vector.

Assuming ρ_S and ρ_G to be the densities of SSDs and GNDs, respectively, the total dislocation density ρ can be expressed as.

$$\rho = \rho_S + \rho_G \tag{2}$$

The GND density and equivalent strain gradient are related by the following relationship:

$$\rho_G = \bar{r}\,\frac{\eta^p}{b} \tag{3}$$

where $\bar{r}$ is the Nye factor used to measure the degree of non-uniform plastic deformation (its value for a face-centered cubic (FCC) crystal is about 1.9 [31]). η^p is the equivalent strain gradient, which is calculated after the material yields.

The relationship between tensile flow-stress and shear flow-stress is as follows:

$$\sigma_F = M\tau = M\alpha\mu b\sqrt{\rho} \tag{4}$$

where M is Taylor factor; M= 3.06 for a FCC material [32].

From Eqs. (1) to (4), we get:

$$\sigma_F = M\alpha\mu b\sqrt{\rho_S + \bar{r}\,\frac{\eta^p}{b}} \tag{5}$$

The contribution of SSDs to the flow stress can be obtained by uniformly deforming a material under uniaxial tensile or compression loading. This is because, under such a condition, ρ_G= 0. In such a scenario, σ_F reduces toσ_F^{1D}, i.e.

$$\sigma_F^{1D} = M\alpha\mu b\sqrt{\rho_S} \tag{6}$$

Thus, ρ_S can be determined from (5) as.

$$\rho_S = \left[\frac{\sigma_F}{M\alpha\mu b}\right]^2 \tag{7}$$

Here, the conventional uniaxial curve is expressed in terms of the equivalent plastic strain in the form of a hardening law. Thus, σ_F^{1D} can be obtained by fitting the uniaxial stress–strain curve; σ_F^{1D} may be related to the SSD density as.

$$\rho_S = \left[\frac{\sigma_{ref} f_p\left(\bar{\varepsilon}^p\right)}{M\alpha\mu b}\right]^2 \tag{8}$$

Substituting Eq. (8) back into (5), one obtains.

$$\sigma_F(e^p, \eta^p) = M\alpha\mu b\sqrt{\left[\frac{\sigma_{ref} f_p\left(\bar{\varepsilon}^p\right)}{M\alpha\mu b}\right]^2 + \bar{r}\,\frac{\eta^p}{b}} \tag{9}$$

where $\eta^p = \sqrt{\frac{1}{4}\eta^p \cdot \eta^p}$ with.

$$\eta^p_{ijk} = \frac{\partial \epsilon^p_{ik}}{\partial x_j} + \frac{\partial \epsilon^p_{jk}}{\partial x_i} - \frac{\partial \epsilon^p_{ij}}{\partial x_k} \tag{10}$$

Based on the above formulas, the flow stress according to the Taylor dislocation model can be expressed as.

$$\sigma_F(e^p, \eta^p) = \sigma_{ref}\sqrt{f_p\left(\bar{\varepsilon}^p\right)^2 + l\eta^p} \tag{11}$$

where l is the intrinsic material length, which depends on the elasticity (μ), plasticity (σ_{ref}), and Burgers vector (b) [33].

$$l = M^2\alpha^2 b\,\bar{r}\,(\mu/\sigma_{ref})^2 \tag{12}$$

Typically, for metals, the Burgers vector b is of the order of 10^{-1} nm, and μ/σ_{ref} is of the order of10^2. Moreover, α is approximately 0.3. This implies that the intrinsic material length is of the order of a micron.

We assume the following isotropic hardening law,

$$\sigma = \sigma_Y\left(1 + \frac{E\bar{\varepsilon}^p}{\sigma_Y}\right)^N \tag{13}$$

The reference stress is defined as $\sigma_{ref} = \sigma_Y(E/\sigma_Y)^N$ and$f_p\left(\bar{\varepsilon}^p\right) = \left(\bar{\varepsilon}^p + \sigma_Y/E\right)^N$.

Moreover, it was assumed that the intrinsic material length did not change during the deformation process. If the characteristic deformation scale of the material is significantly larger than the intrinsic material length, the strain gradient term $l\eta^p$ in formula (11) can be ignored, and, consequently, the flow stress reduces to that of the classical elastic–plastic theory, i.e.,$\sigma_F = \sigma_{ref} f_p(\bar{\varepsilon}^p)$.

2.2. Calculation of the plastic strain gradient

The discrete gradient method proposed by Liszka and Orkisz [34] was adopted for the strain gradient calculation. First, the plastic strain rate was assumed to be a sufficiently differentiable

function, i.e.,$\dot{\varepsilon}_{ij}^{p}(\boldsymbol{r})$. The first-order Taylor series expansion around point $\boldsymbol{r}_0 = \{x_0, y_0\}$ is.

$$\dot{\varepsilon}_{ij}^{p}(r) = \dot{\varepsilon}_{ij}^{p}(r_0) + \Gamma \cdot \Delta r + O(\Delta^2) \tag{14}$$

where $\boldsymbol{\Gamma}$ represents the unknown gradient vector, i.e.

$$\Gamma = \{\dot{\varepsilon}_{ij,1}^{p}(r_0), \dot{\varepsilon}_{ij,2}^{p}(r_0)\}^{\top} \tag{15}$$

In Eq. (14), $\Delta \boldsymbol{r}$ is defined as $\Delta r = \{\Delta x, \Delta y\}^{\top}$ with$\Delta x = x - x_0, \Delta y = y - y_0$. And$\Delta^2 = \Delta x^2 + \Delta y^2$. A set of linear equations can be derived by writing Eq. (14) for each Gauss point around a central Gauss point where the gradient is to be realized. Since the number of such Gauss points n is unknown, the equations processed are integrated into an overdetermined linear system to increase approximation accuracy. Hence, the solution requires a minimization procedure. For this purpose, we define a function f such that.

$$f(\Gamma) = \sum_{k=1}^{n} \left[\frac{\dot{\varepsilon}_{ij}^{\rho}(r_0) - \dot{\varepsilon}_{ij}^{p}(r_k) + \Gamma \cdot \Delta r_k}{\Delta_k^3}\right]^2 \tag{16}$$

where $1 / \Delta_k^3$ denotes the weighting factor. The desired gradients were determined by minimizing $f(\boldsymbol{\Gamma})$ using$\partial f / \partial \boldsymbol{\Gamma} = 0$. The USDFLD subroutine found in the ABAQUS software was used for this purpose.

It must be mentioned that during the calculation of the gradient at a point i, all the Gauss points in the model were not used since that would have required significant storage and computing power. Instead, as shown in Fig. 3, an interaction radius R was defined, and the Gauss points within the interaction radius were used to calculate the gradient at point i. Gradient calculations at the Gauss points were conducted at the end of each step and finite increment of the plastic strain. Subsequently, the calculated gradients were passed back to the main constitutive calculation module.

3. Materials and experimental methods

Chemical or structural gradients are introduced into engineering materials to improve their mechanical properties [35]. The introduction of structural gradients can overcome the performance limitations of traditional material systems, alleviate stress concentration, and produce specific functions.

In the present study, the metallic materials with tunable structural gradients were prepared using the concept of bottom-up manufacturing, which had been reported in our previous work [36]. This allows the mode and sequence of the gradient structure to be arbitrarily controlled. First, different types of metal sheets were prepared using the ball-milling method. Sheets, several hundred nanometers thick, were evenly mixed in an ethanol medium and then filtered under vacuum. The composite powder assembly process allowed us to accurately adjust the layer composition

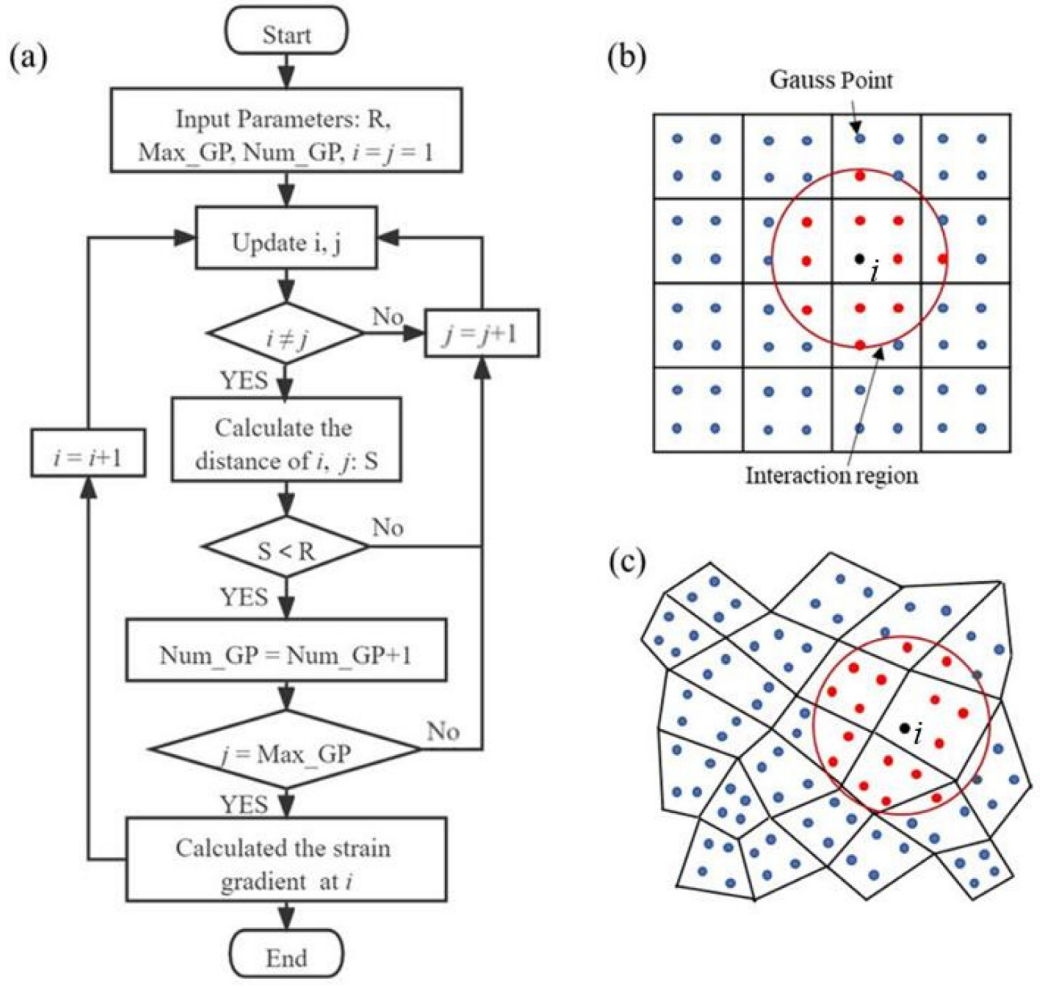

Fig. 3. Calculation of strain gradient (Num_GP: the number of Gauss points within the Interaction region; Max_GP: the total number of Gauss points): (a) flowchart for the calculation of the strain gradient calculation, (b) gradient calculation at point i (regular finite element mesh), (c) gradient calculation at point i (Irregular finite element mesh).

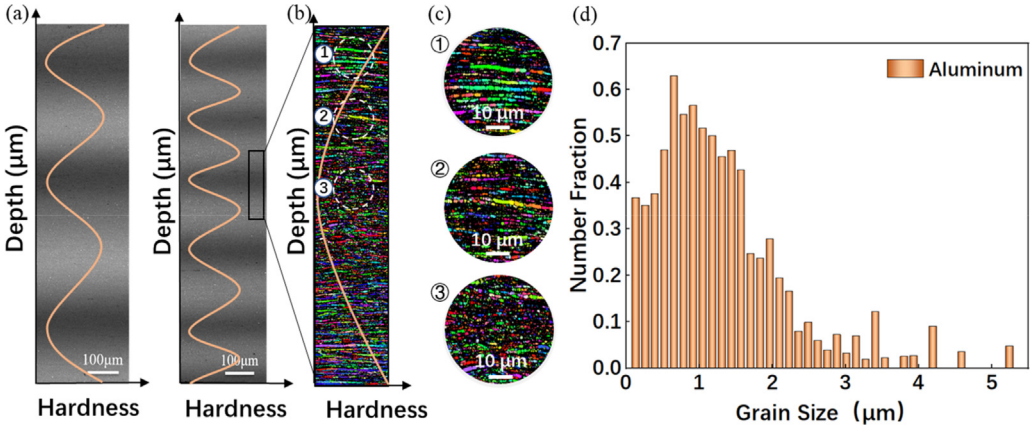

Fig. 4. Microstructure of the heterostructured bulk aluminum (Al/7055): (a) backscatter electron (BSE) images and hardness of periodic gradient materials with three cycles (GC3) and six cycles (GC6), (b) electron backscattered diffraction (EBSD) images of one cycle GC6, (c) enlarged views of some of the regions of the EBSD image, and (d) grain size distribution plot.

and thickness. In this study, we used 7055 aluminum alloy and pure aluminum (99.9% purity) for the hard and soft regions, respectively, and obtained a transition zone by changing their relative proportions. For this, combinations of 75% aluminum alloy + 25% pure aluminum, 50% aluminum alloy + 50% pure aluminum, and 25% aluminum alloy + 75% pure aluminum were used.

Backscatter electron (BSE) and electron backscattered diffraction (EBSD) were used to characterize the microstructure of the heterogeneous material. Fig. 4a shows the BSE images of the materials with three cycles (GC3) and six cycles (GC6) and the corresponding hardness distribution. The absence of sharp interface in BSE image is attributed to the elemental diffusion upon hot working [36]. Fig. 4b shows the grain orientation distribution of the GC6 material with one cycle wherein the microstructure is regularly distributed with a change in the hardness, grains with sizes below ~ 150 nm cannot be resolved by EBSD probably due to large residual stress in the as-fabricated samples. Based on the processing technique and EBSD image, we believe that the large-grained strips are mainly composed of the 7055 aluminum alloy. Fig. 4c shows enlargement of grains with approximately 100% aluminum alloy, 50% aluminum alloy + 50% aluminum alloy, and 100% aluminum in the three locations. As shown in Fig. 4d, the grain size measured by EBSD varies between 1 and 2 μm. It is necessary to consider the strain gradient plasticity and intrinsic material length during deformation.

4. Microstructural modeling

To obtain the material parameters for the simulation, the mechanical responses of the hard and soft phases were studied using micropillar compression tests. For this, pure aluminum and 7055 aluminum alloy micropillars with a diameter of 2 μm and a

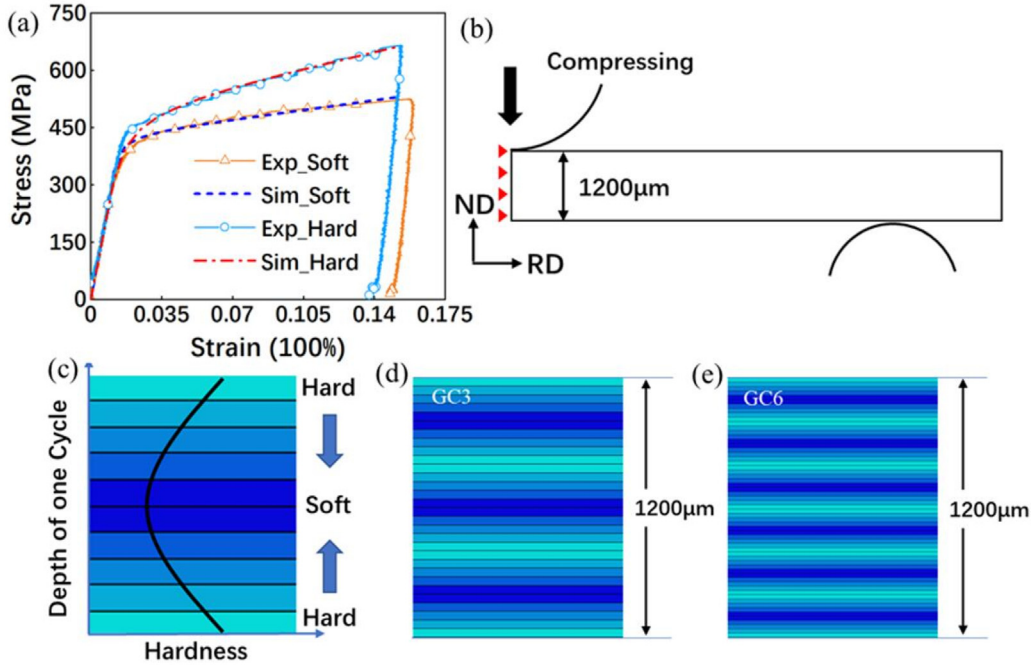

Fig. 5. (a) Experimentally obtained and simulated stress–strain curves of the hard (7055) and soft (Al) phases. (b) Finite element model for bending tests. (c) One-cycle material model schematic (Transitioning from the hard phase aluminum alloy 7055 to the soft phase Al and then to the hard phase). (d) Schematic of a material model with three gradient cycles (GC3). (e) Schematic of a material model with six gradient cycles (GC6).

height of 6 μm were prepared using a focused ion beam (FIB, FEI Scios) and were then compressed at a strain rate of 5×10^{-4} s^{-1} under a nanometer informer with a flat punch tip. Continuous stiffness measurement (CSM) was used to monitor the change in contact stiffness during the compression test at a harmonic frequency of 75 Hz and an amplitude of 2 nm. The true stress and true strain were obtained by dynamically recording the load and displacement of the head according to the method developed by Greer et al. [37]. Fig. 5a shows the stress–strain diagrams obtained both from the test and the simulation. The obtained elastic modulus, yield stress, hardening exponent and strain gradient theory related parameter of the soft phase (Al) were E = 54 GPa, Y = 400 MPa, N = 0.03, M = 3.06, $\bar{r}$ = 1.9, and l = 0.05 μm, respectively. For the hard phase (7055 alloy), the corresponding values were E = 50 GPa, Y = 450 MPa, N = 0.09, M = 3.06, $\bar{r}$= 1.9, and l = 0.05 μm. Although the elastic modulus increases due to compression, such a change was ignored and, instead, the initial elastic moduli were used.

The effects of the number of periods and stress distribution as well as the distribution of GNDs between two adjacent layers were studied using finite element simulations. Three-point bending simulations were performed using ABAQUS/Standard [38] combined with the user subroutine module (UMAT + USDFLD). To better study the effect of the strain gradient along the depth of the material, a 2D plane-strain geometric model was used for the simulations. The gradient structure of the material in the thickness direction was represented by an ideal model of uniform layer transitions [27,39]. As shown in Fig. 5a, the parameters of the hard and soft phases were inverted. The properties of each layer were interpolated and matched to those of the real material according to the ratio of soft and hard phases in them. Fig. 5c–e show schematics of the material model with one, three, and six cycles, respectively.

5. Results and discussion

5.1. Macroscopic mechanical behavior

The role of GNDs in mechanical responses is explained by the mechanism-based strain gradient plasticity. The extra hardening behavior can be reflected by geometrical dislocations by changing intrinsic material lengths (l). Effects of a change in the intrinsic material length scale was studied with the GC3 material model. The intrinsic material lengths used for this purpose were (i) l = 0 μm, (ii) l = 0.05 μm, (iii) l = 0.1 μm, and (iv) l = 0.15 μm, and the results are shown in Fig. 6.

Two observations could be made from Fig. 6. First, the mechanical response with the inclusion of GNDs shows a higher strength than the conventional plastic case (l = 0). Second, the strength of the material is directly correlated to the magnitude of l.

Three-point bending tests were performed on specimens GC3 and GC6. The test specimens were 1.2 mm thick and 3 mm wide. The span between two consecutive support points was 20 mm. And the radius of the indenter was 1.5 mm. For comparison, bending simulations on the corresponding two material models with similar conditions were also conducted. In addition to this, bending simulations were also performed on material models with the properties of pure Al and 7055 Al alloy. The results are shown in Fig. 7. Based on this, it can be observed that gradient materials exhibit excellent mechanical properties, which is consistent with previous experiments [36]. In particular, the strength of GC3 was higher that of pure aluminum. Moreover, when the material cycle was increased to six cycles, its strength became similar to that of 7075 Al alloy. In addition to this, it was observed that, for the same ratio of the soft and hard phases, the greater is the dislocation density accumulated during the deformation process, the higher the strength of the material.

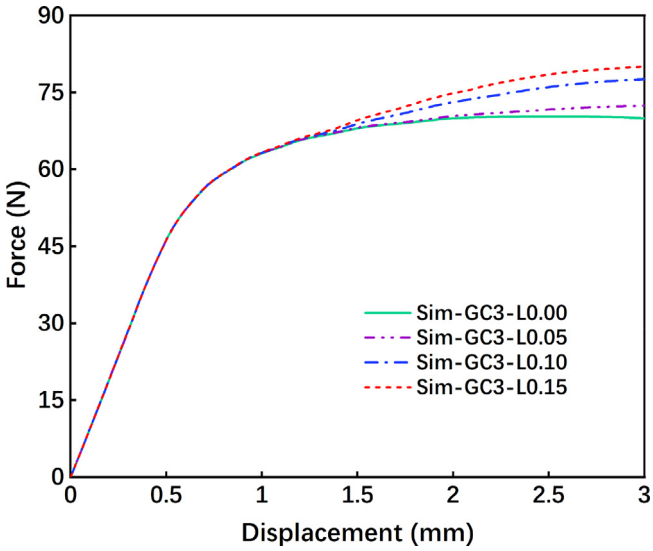

Fig. 6. Influence of intrinsic material length on the macroscopic mechanical behavior studied using the Taylor dislocation model.

5.2. Micromechanical behavior

For a given material thickness, the number of cycles is one of the main factors affecting the performance of controllable gradient materials. Three-point bending simulations were carried out using two material models with different numbers of cycles (GC3/GC6) but with the same overall size. Owing to the different number of gradient periods, model with more cycles has smaller transition layer thicknesses for the same material size. In this section, we discuss the plastic deformation behavior of homogeneous materials (pure 7055 Al alloy), GC3, GC6, and the characteristics of the Taylor strengthening mechanism. Fig. 8 shows the strain distribution cloud diagram of the three material models under different deflections.

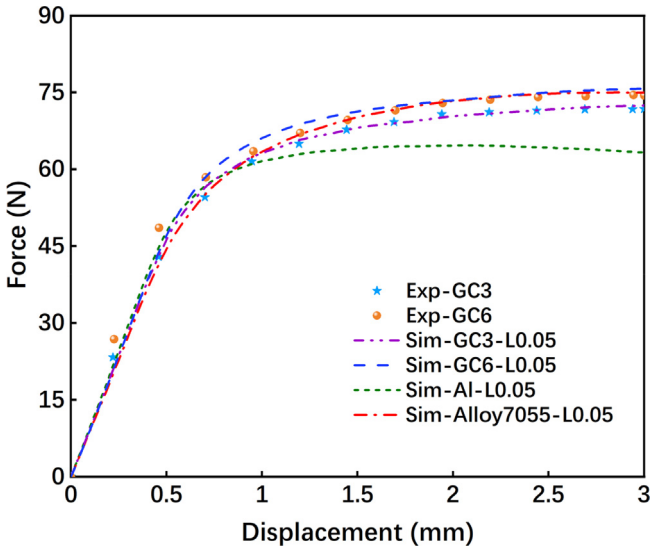

Fig. 7. Simulation and Experiment: force–displacement curve.

With an increase in the deflection from 1 mm to 3 mm, the strains at the bottom of GC3 and GC6 became uneven. In contrast, even though the corresponding strain in the single-phase material increased with an increase in the deflection, it remained even. In addition, it can be observed that the strain distribution is related to the number of cycles. When the bending deflection was 2 mm, an unevenness in the strain distribution at the bottom of GC3 appeared to have initiated whereas it was fully developed in the case of GC6. To further study the distribution of strain in the bulk of the material, strain values within a depth of 600 μm to 1200 μm (neutral axis and below) were extracted from the surface. Fig. 9 shows the variation of these strains with depth in the three models under different deflections.

At 1 mm deflection, strains in all the three models increased in a perfectly linear manner with depth. Next, when the deflection increased to 2 mm, the variation in the strain in GC6 showed significant fluctuation whereas the fluctuation was minor in GC3. Ultimately, when the deflection was increased to 3 mm, the strain distributions in both GC3 and GC6 fluctuated considerably, and the amount of fluctuation was higher in GC6. The above results indicate that the periodic gradient structure of the material affects the strain distribution and, unlike in the case of a single phase material, prevents the deformation from proceeding evenly. The uneven strain distribution is conducive to the generation of dislocations, thus providing an additional strengthening effect and increasing the work-hardening capacity of the material.

Mathematically, the strain gradient of the slip system is closely related to dislocations. Fig. 10a and 10b show the distribution of GND in GC3 and GC6. Fig. 10c and 10d show the variation in the GND density with depth. It is clear from these figures that the distribution of GND is also strongly correlated to the microstructure of the material.

The distribution of GNDs were observed to be relatively more uniform in GC6. As shown in Fig. 10c, the number of peaks in the GND distribution increases with an increase in the number of layers. Upon calculating the mean GND density in GC6 and GC3, it was observed that increasing the number of cycles from three to six is beneficial for generating more strain gradient and increasing the

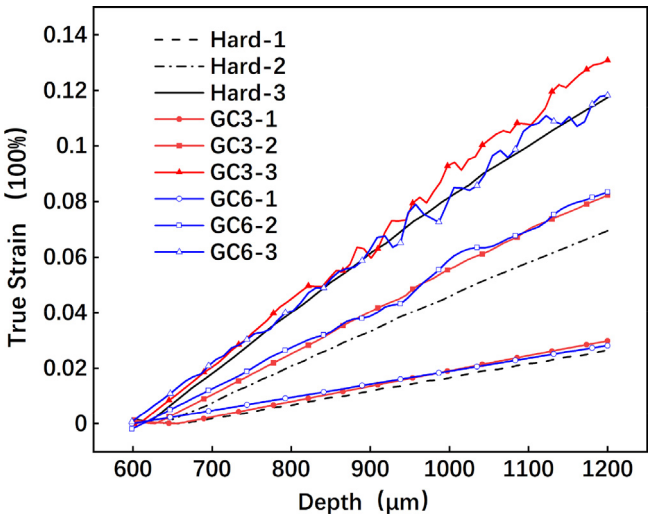

Fig. 9. Variation of strain with depth in single phase, GC3, and GC6 at different deflections.

average density of GND, which results in a significant improvement in the strength.

The constituents of periodic gradient materials form a gradient structure that then periodically repeats across the sample. Fig. 10d shows the variation of GND density with distance from the neutral axis both within a period and across layers in GC6. The existence of a double gradient provides new possibilities for obtaining materials with exceptional mechanical properties.

The distribution of GND in the fabricated materials was also studied. For this, the analysis tool for electron and X-ray diffraction (ATEX) [40] was used to process the EBSD data and obtain the GND map. In this process, Burges vector length of aluminum was used for calculate GND density. And the magnitude of Burgers vector b is approximately 0.286 nm [28]. As shown in Fig. 11a, the obtained GND distribution map was divided into fifty equal regions, and the values at five random points with relatively concentrated GNDs

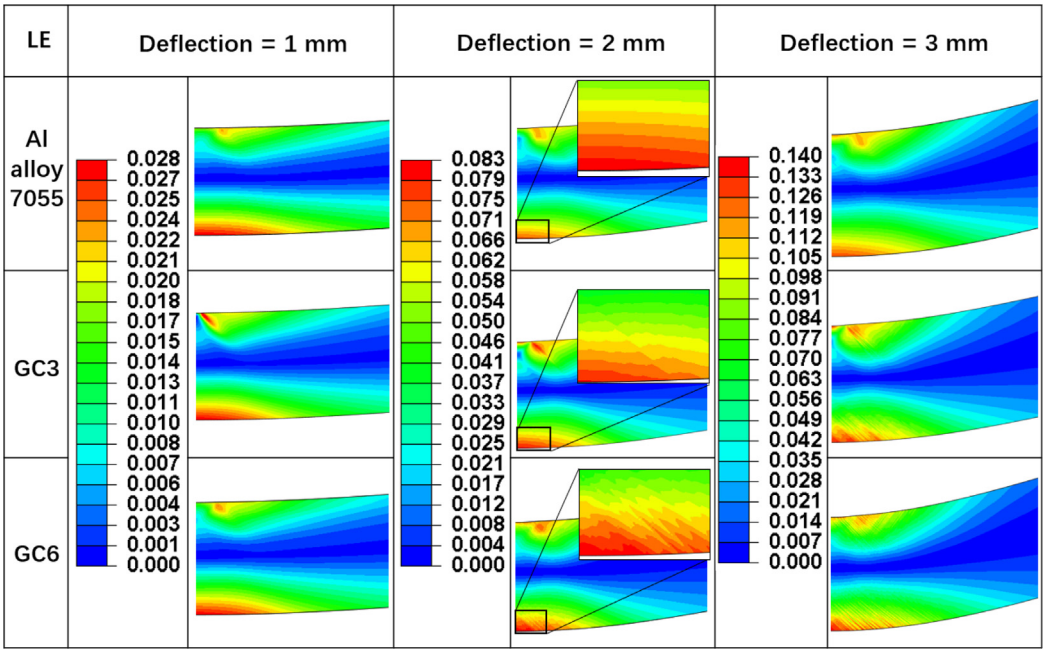

Fig. 8. Strain distribution maps of single phase (hard), GC3, and GC6 at different deflections.

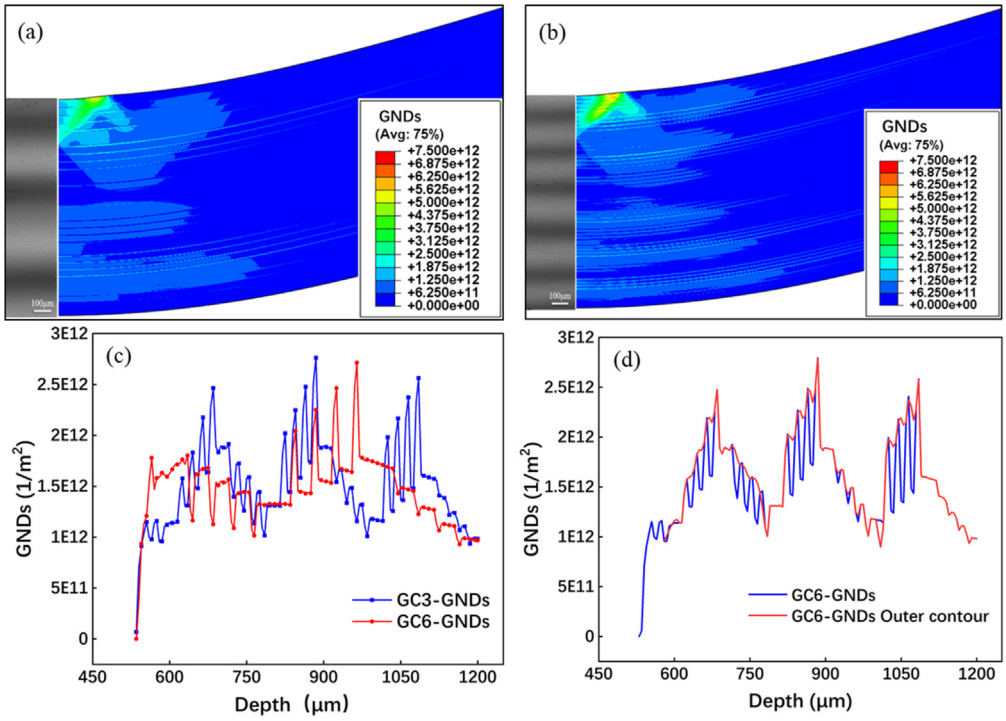

Fig. 10. GND distribution in heterostructured bulk Al with controllable gradient structure. (a) three cycle gradient (GC3) and (b) six cycle gradient (GC6). (c) Variation in the GNDs density with depth in GC3 and GC6. (d) Dual gradient effect in periodic gradient materials.

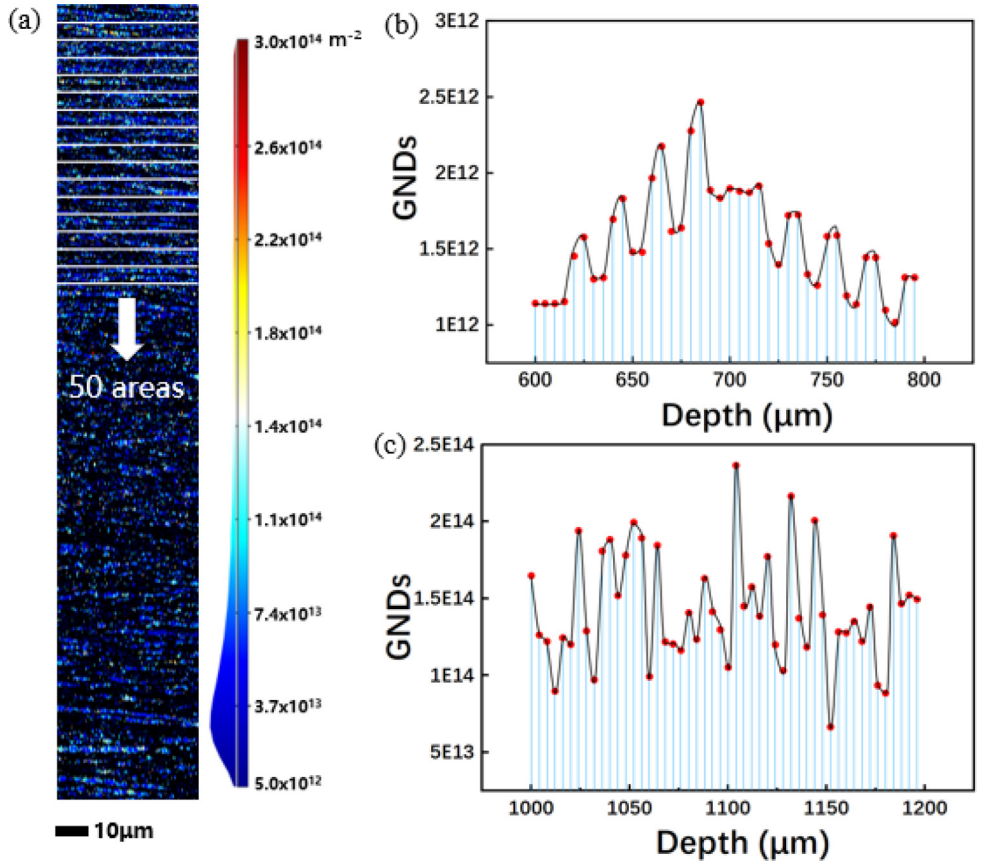

Fig. 11. (a) GND distribution map divided into fifty regions. (b) Variation of GND density with depth obtained from the simulation results. (c) Variation of GND density with depth direction obtained from the EBSD results.

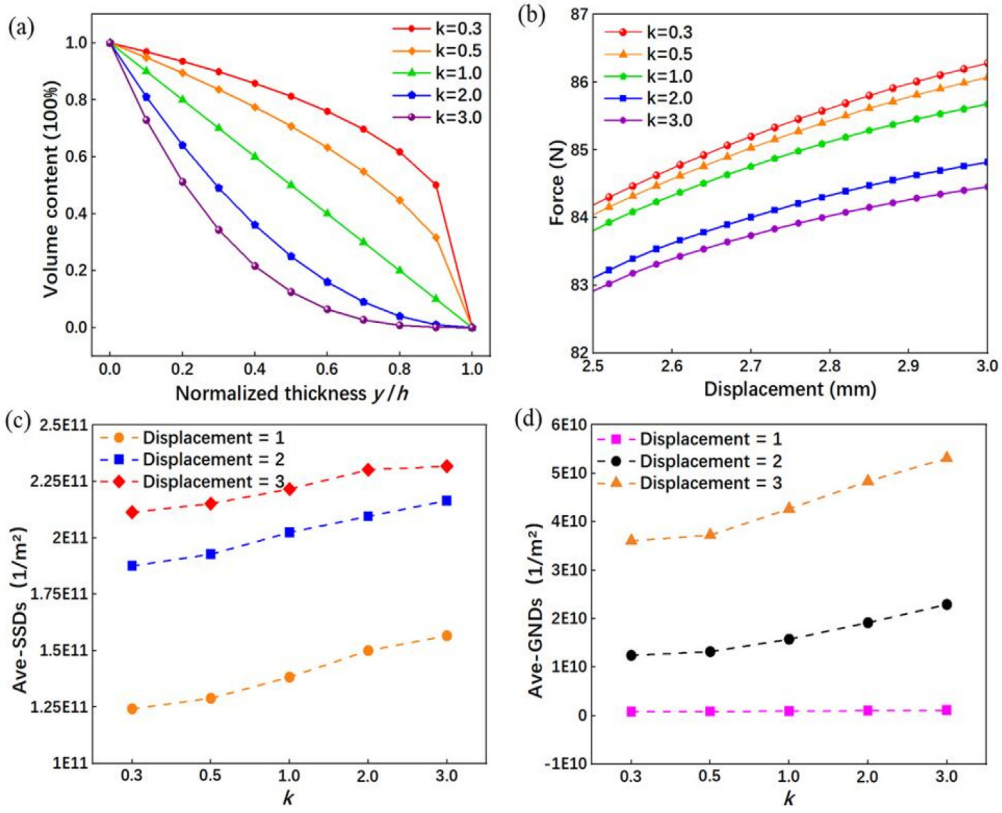

Fig. 12. (a) Variation in the volume fraction of the hard phase with depth (Y-axis). (b) The influence of *k* to force–displacement curve. (c) Average SSD density. (d) Average GND density.

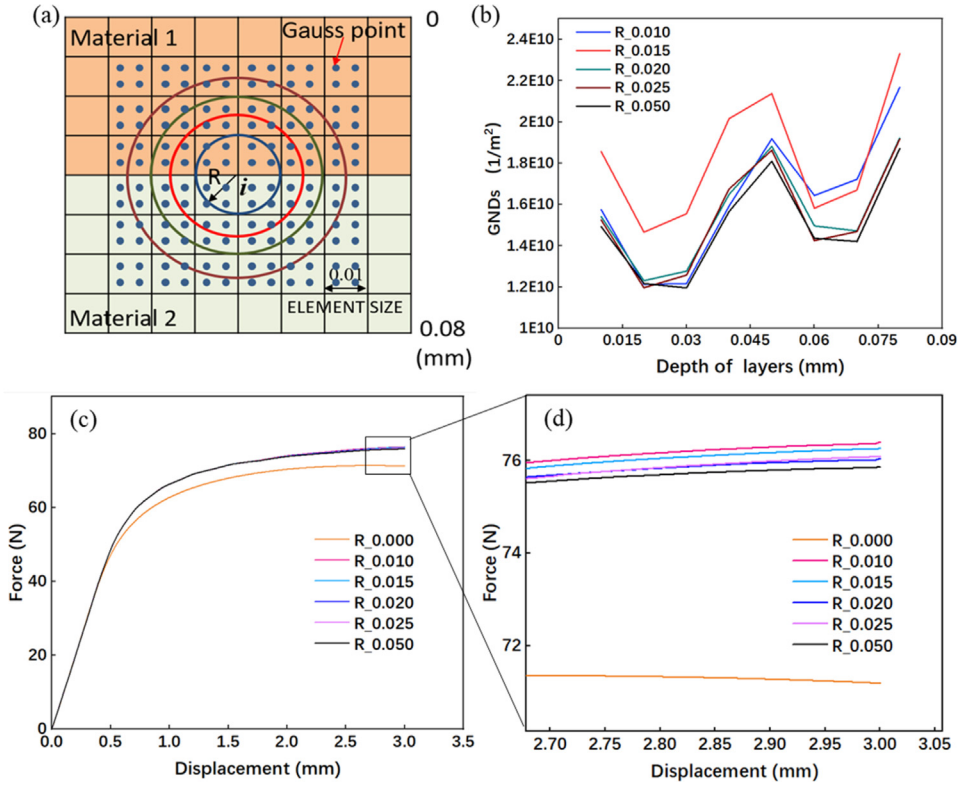

Fig. 13. (a) Schematic of the interaction radius *R*. (b) Variation of the geometrically necessary dislocation density between the two layers of the material. (c) Bending force–displacement curves corresponding to different interaction radii (*R*). (d) Magnified view of a portion of the force–displacement curve.

were selected from each region to obtain the corresponding mean GND density.

Fig. 11b and 11c show the variation of GND density with depth in GC6 obtained from the finite element simulations and the EBSD data, respectively. Therein, it can be observed that the GND density fluctuates with depth in both the simulation and experimental results. GNDs in Fig. 11c does not have a gradient distribution as the simulation results, and is not strictly increased first and then decreased. This may be due to the fact that the material has been rolled and hardened before bending. Thus, the hardness difference ratio of each layer is reduced. Notably, the GND density obtained from the EBSD results is approximately two orders of magnitude higher. This is due to the fact that dislocations generated during material preparation were not considered in the simulations. However, the effect is reflected in the material parameters obtained by compression experiments.

5.3. Gradient design of heterostructured bulk Al

The change in the volume fraction distribution of the soft and hard phases affects the mechanical properties of gradient structured materials. The experimental and simulated models showed linear changes in the material volume fraction. The heterogeneous gradient gradually varied from 100% 7055 Al alloy to 100% pure Al with depth (Y-axis). The volume fraction of the hard phase is given by.

$$V_H = \left(1 - \frac{y}{h}\right)^k \tag{17}$$

where k is the volume fraction index, h is the thickness of material.

A bending simulation was performed on the heterogeneous aluminum with one cycle. Fig. 12a shows the variation in the volume fraction of the hard phase with depth for different values of k. From this, it can be observed that with an increase in the value of k, volume fraction of the hard phase decreases. As shown in Fig. 12b, the material model with a larger value of k had a lower strength, but the difference was not as large as that obtained from ROM. In other words, when the value of k is higher, despite its lower intensity. But stronger dislocation reinforcement makes up for the strength gap due to different hard phase volume fractions. Fig. 12c and 12d show variation of the SSD and GND densities averaged over the entire bending model with k at different bending deflections. From these results, it can be said that an increase in the volume fraction index of the hard phase results in an increase in the dislocation density, which further contributes to the material stress.

6. Conclusion

In this study, the mechanical properties of heterostructured bulk aluminum (Al/7055) with three and six gradient cycles were investigated. Their microstructures were characterized by electron backscattered diffraction, and the distribution of geometrically necessary dislocations along the thickness of the material was investigated and discussed through numerical simulations. The selection of the intrinsic material length and influence of the recently developed gradient calculation method on the simulation results were also studied. The following conclusions could be drawn:

- Disregarding the change in the intrinsic length scale of the materials results in a significant difference in the macroscopic response. To accurately describe the gradient effect in gradient structure materials, the intrinsic gradient of the length-scale parameters must be considered.
- The introduction of a gradient structure in metal matrix composites results in inhomogeneous deformation across the different layers, and the induced strain gradient can help improve the amount of work hardening. Through bending tests and simulations, we found that the number of material gradient cycles had a direct influence on the mechanical response.
- GNDs were found to accumulate at the interface between the metal matrix and the reinforcement. Moreover, modification of the microstructure by incorporating a periodic structure helped achieve large-scale strain gradient across the material. This double strain-gradient effect provides a basis for the preparation of composite materials.
- To study the influence of the change of phase volume fraction on mechanical properties, a distribution equation was proposed for the hard and soft phases in the form of the volume fraction exponent. The simulation results show that the dislocation density increases when the volume fraction of the harder phase is less.

CRediT authorship contribution statement

Xihang Zhao: . **Zhenming Yue:** Writing – review & editing, Supervision, Project administration. **Ge Wang:** . **Zan Li:** Writing – review & editing. **Celal Soyarslan:** .

Declaration of Competing Interest

The authors declare that they have no known competing financial interests or personal relationships that could have appeared to influence the work reported in this paper.

Acknowledgment

This work was supported by the National Natural science foundation of China (Nos.52175337, 52192591 and 52171142)

Appendix

Heterostructured aluminum with a controllable gradient structure was prepared using the powder assembly method. The percentage of hard and soft phases in the two adjacent layers were different. The other mechanical properties were then reflected. In addition, it balances the strength and toughness of the material. To study the distribution of dislocations in two adjacent layers, we extracted a part of the model containing two layers of components in one cycle. Different interaction radii (R) were selected to control the size of the gradient, and their influence on the numerical simulation was studied. As shown in Fig. 13a, the number of Gauss points included in the gradient calculation is dependent on the value of R. However, the disadvantage of using a larger radius is that more material components would have to be included. After the weighted average, the difference in the strain gradient may be offset, and the distribution tends to be averaged, which is not desired. On the other hand, the number of Gauss points obtained by using a small value of R is insufficient to account for the influence region around the deformed region.

The weighted average method we used solves this problem, and the influence of the radius on the result converges to the desired range.

As shown in Fig. 13b, upon increasing the value of the interaction radius initially equivalent to the size of one element to that of five elements, GND density first increases and then decreases. Convergence is achieved only when the interaction radius lies between 2 and 2.5 times the element size. Accordingly, the GND density thus evaluated first increases with depth until it reaches the

interface (where its value is maximum) and then decreases owing to the transition to the next layer.

Fig. 13c shows the influence of the interaction radius on the macroscopic properties of the material. When R = 0, i.e., strengthening due to GNDs is ignored, the force required to bend the material decreases significantly. When R lied between 0.01 and 0.05, the influence was similar to that of GNDs, and all the curves seemed to coincide with minor variation amongst them.

References

[1] Y. Wei, Y. Li, L. Zhu, Y. Liu, X. Lei, G. Wang, Y. Wu, Z. Mi, J. Liu, H. Wang, H. Gao, Evading the strength-ductility trade-off dilemma in steel through gradient hierarchical nanotwins, Nat Commun. 5 (1) (2014), https://doi.org/10.1038/ncomms4580.

[2] XiaoLei Wu, P. Jiang, L. Chen, F. Yuan, Y.T. Zhu, Extraordinary strain hardening by gradient structure, Proc Natl Acad Sci U S A. 111 (20) (2014) 7197–7201.

[3] C.F. Niordson, J.W. Hutchinson, On lower order strain gradient plasticity theories, Eur J Mech a-Solid. 22 (6) (2003) 771–778.

[4] P. Gudmundson, A unified treatment of strain gradient plasticity, J Mech Phys Solids. 52 (6) (2004) 1379–1406.

[5] J.L. Bassani, Incompatibility and a simple gradient theory of plasticity, J Mech Phys Solids 49 (9) (2001) 1983–1996.

[6] E. Ma, X. Wu, Tailoring heterogeneities in high-entropy alloys to promote strength–ductility synergy, Nat Commun 10 (1) (2019), https://doi.org/10.1038/s41467-019-13311-1.

[7] Z. Cheng, H. Zhou, Q. Lu, H. Gao, L. Lu, Extra strengthening and work hardening in gradient nanotwinned metals, Science. 362 (6414) (2018), https://doi.org/10.1126/science:aau1925.

[8] H. Wu, M. Huang, Q. Li, J. Wu, J. Li, Z. Wang, G. Fan, Manipulating the plastic strain delocalization through ultra-thinned hierarchical design for strength-ductility synergy, Scr Mater. 172 (2019) 165–170.

[9] H.W. Huang, Z.B. Wang, J. Lu, K. Lu, Fatigue behaviors of AISI 316L stainless steel with a gradient nanostructured surface layer, Acta Mater. 87 (2015) 150–160.

[10] T.H. Fang, W.L. Li, N.R. Tao, K. Lu, Revealing extraordinary intrinsic tensile plasticity in gradient nano-grained copper, Science. 331 (6024) (2011) 1587–1590.

[11] X.L. Wu, P. Jiang, L. Chen, J.F. Zhang, F.P. Yuan, Y.T. Zhu, Synergetic Strengthening by Gradient Structure, Mater Res Lett. 2 (4) (2014) 185–191.

[12] J. Zhao, X. Lu, F. Yuan, Q. Kan, S. Qu, G. Kang, X.u. Zhang, Multiple mechanism based constitutive modeling of gradient nanograined material, Int J Plast. 125 (2020) 314–330.

[13] Y. Zhu, J. Woody Ju, Interface energy effect on effective elastic moduli of spheroidal particle-reinforced nanocomposites, Acta Mech. 231 (7) (2020) 2697–2709.

[14] Y. Zhu, X. Wu, Perspective on hetero-deformation induced (HDI) hardening and back stress, Mater Res Lett. 7 (10) (2019) 393–398.

[15] X. Li, L. Lu, J. Li, X. Zhang, H. Gao, Mechanical properties and deformation mechanisms of gradient nanostructured metals and alloys, Nat Rev Mater. 5 (9) (2020) 706–723.

[16] M.F. Ashby, The deformation of plastically non-homogeneous materials, The Philosophical Magazine: A Journal of Theoretical Experimental and Applied Physics. 21 (170) (1970) 399–424.

[17] Y. Zhu, K. Ameyama, P.M. Anderson, I.J. Beyerlein, H. Gao, H.S. Kim, E. Lavernia, S. Mathaudhu, H. Mughrabi, R.O. Ritchie, N. Tsuji, X. Zhang, X. Wu, Heterostructured materials: superior properties from hetero-zone interaction, Mater Res Lett. 9 (1) (2021) 1–31.

[18] Y. Estrin, Y. Beygelzimer, R. Kulagin, P. Gumbsch, P. Fratzl, Y. Zhu, H. Hahn, Architecturing materials at mesoscale: some current trends, Mater Res Lett. 9 (10) (2021) 399–421.

[19] J.S. Stölken, A.G. Evans, A microbend test method for measuring the plasticity length scale, Acta Mater. 46 (14) (1998) 5109–5115.

[20] A.G. Evans, J.W. Hutchinson, A critical assessment of theories of strain gradient plasticity, Acta Mater. 57 (5) (2009) 1675–1688.

[21] N.A. Fleck, G.M. Muller, M.F. Ashby, J.W. Hutchinson, Strain Gradient Plasticity - Theory and Experiment, Acta Metallurgica Et Materialia. 42 (2) (1994) 475–487.

[22] Chong ACM, Lam DCC. Strain gradient plasticity effect in indentation hardness of polymers. 2015.

[23] J. Li, G.J. Weng, S. Chen, X. Wu, On strain hardening mechanism in gradient nanostructures, Int J Plast. 88 (2017) 89–107.

[24] J. Li, A.K. Soh, Modeling of the plastic deformation of nanostructured materials with grain size gradient, Int J Plast. 39 (2012) 88–102.

[25] X. Lu, X.u. Zhang, M. Shi, F. Roters, G. Kang, D. Raabe, Dislocation mechanism based size-dependent crystal plasticity modeling and simulation of gradient nano-grained copper, Int J Plast. 113 (2019) 52–73.

[26] J. Zhao, Q. Kan, L. Zhou, G. Kang, H. Fan, X.u. Zhang, Deformation mechanisms based constitutive modelling and strength-ductility mapping of gradient nano-grained materials, Mater Sci Eng A Struct Mater. 742 (2019) 400–408.

[27] Y. Zhang, Z. Cheng, L. Lu, T. Zhu, Strain gradient plasticity in gradient structured metals, J Mech Phys Solids. 140 (2020) 103946, https://doi.org/10.1016/j.jmps.2020.103946.

[28] H. Gao, Y. Huang, Taylor-based nonlocal theory of plasticity, Int J Solids Struct. 38 (15) (2001) 2615–2637.

[29] Y. Huang, S. Qu, K.C. Hwang, M. Li, H. Gao, A conventional theory of mechanism-based strain gradient plasticity, Int J Plast. 20 (4-5) (2004) 753–782.

[30] W. D. Nix, Elastic and plastic properties of thin films on substrates: nanoindentation techniques, Mater Sci Eng A Struct Mater. 234-236 (1997) 37–44.

[31] A. Arsenlis, D.M. Parks, Crystallographic aspects of geometrically-necessary and statistically-stored dislocation density, Acta Mater. 47 (5) (1999) 1597–1611.

[32] J.F.W. Bishop, R. Hill C.X.X.V.I.I.I., A theoretical derivation of the plastic properties of a polycrystalline face-centred metal. The London, Edinburgh, and Dublin Philosophical Magazine and Journal of, Science. 42 (334) (2012) 1298–1307.

[33] N.A. Fleck, J.W. Hutchinson, A Phenomenological Theory for Strain Gradient Effects in Plasticity, J Mech Phys Solids. 41 (12) (1993) 1825–1857.

[34] T. Liszka, J. Orkisz, The Finite-Difference Method at Arbitrary Irregular Grids and Its Application in Applied Mechanics, Comput Struct. 11 (1-2) (1980) 83–95.

[35] T.P.D. Rajan, B.C. Pai, Developments in Processing of Functionally Gradient Metals and Metal–Ceramic Composites: A Review, Acta Metall. Sin. (Engl. Lett.) 27 (5) (2014) 825–838.

[36] G.e. Wang, H. Ouyang, Y. Su, Q. Guo, D.-B. Xiong, Q. Zhuang, Z. Yue, Z. Li, D.i. Zhang, Heterostructured bulk aluminum with controllable gradient structure: Fabrication strategy and deformation mechanisms, Scr Mater. 196 (2021) 113762, https://doi.org/10.1016/j.scriptamat.2021.113762.

[37] J.R. Greer, W.C. Oliver, W.D. Nix, Size dependence of mechanical properties of gold at the micron scale in the absence of strain gradients, Acta Mater. 53 (6) (2005) 1821–1830.

[38] ABAQUS/Standard User's Manual Version 6.3, 2002. Hibbit, Karlsson and Sorensen Inc.

[39] T.V. Mathew, S. Natarajan, E. Martinez-Paneda, Size effects in elastic-plastic functionally graded materials, Compos Struct. 204 (April) (2018) 43–51.

[40] B. Beausir JJF. Analysis Tools for Electron and X-ray diffraction, ATEX - software, www.atex-software.eu, Université de Lorraine - Metz. 2017.